LETTER

Cessation of CCL2 inhibition accelerates breast cancer metastasis by promoting angiogenesis

Laura Bonapace[1,2]*, Marie-May Coissieux[1]*, Jeffrey Wyckoff[1]†, Kirsten D. Mertz[3,4], Zsuzsanna Varga[3], Tobias Junt[2]* & Mohamed Bentires-Alj[1]*

Secretion of C–C chemokine ligand 2 (CCL2) by mammary tumours recruits CCR2-expressing inflammatory monocytes to primary tumours and metastatic sites, and CCL2 neutralization in mice inhibits metastasis[1] by retaining monocytes in the bone marrow. Here we report a paradoxical effect of CCL2 in four syngeneic mouse models of metastatic breast cancer. Surprisingly, interruption of CCL2 inhibition leads to an overshoot of metastases and accelerates death. This is the result of monocyte release from the bone marrow and enhancement of cancer cell mobilization from the primary tumour, as well as blood vessel formation and increased proliferation of metastatic cells in the lungs in an interleukin (IL)-6- and vascular endothelial growth factor (VEGF)-A-dependent manner. Notably, inhibition of CCL2 and IL-6 markedly reduced metastases and increased survival of the animals. CCL2 has been implicated in various neoplasias and adopted as a therapeutic target[1–3]. However, our results call for caution when considering anti-CCL2 agents as monotherapy in metastatic disease and highlight the tumour microenvironment as a critical determinant of successful anti-metastatic therapy.

Most breast-cancer-related deaths are caused by metastases in vital organs. The tumour microenvironment is key for cancer growth, dissemination and metastasis[4–6]. A high number of intratumoral macrophages correlates with poor prognosis[1,7–12] and macrophage infiltration in breast cancer correlates with high expression of the monocyte chemoattractant CCL2. CCL2 has been proposed as a target for metastatic breast cancer because high expression of CCL2 correlates with a decrease in survival of breast cancer patients[10,11,13,14] (Extended Data Fig. 1a, b), and because monocytes expressing the CCL2 receptor enhance metastasis via VEGF secretion in mice[1,15].

We assessed the effect of CCL2 neutralization on tumour growth and metastasis in syngeneic mouse models of CCL2-secreting metastatic breast cancer (Extended Data Fig. 1c–e). Although anti-CCL2 treatment had no effect on primary tumour growth, it reduced the number of lung metastases (Extended Data Fig. 2a–c) and circulating tumour cells (CTCs) (Extended Data Fig. 2d). Intravital imaging[16] showed that anti-CCL2 treatment reduced cancer cell motility and blood vessel leakiness in the tumour, and we found more pericytes around blood vessels (Extended Data Fig. 2e–g and Supplementary Videos 1, 2). Decreased blood vessel leakiness upon anti-CCL2 treatment correlated with fewer CTCs and reduced intratumoral macrophage numbers (Extended Data Fig. 3a, b). Therefore, CCL2 neutralization limits metastases not only through effects on pre-metastatic niches[1] but also by limiting cancer cell intravasation.

Next we examined the persistence of the anti-metastatic effect of CCL2 neutralization after treatment was discontinued. The antibody was cleared within 10 days after treatment (Extended Data Fig. 3c), leading to a rebound of CCL2 in the lungs (Extended Data Fig. 1e). Surprisingly, we found that cessation of anti-CCL2 treatment accelerated death (Fig. 1a). Ten days after interruption of anti-CCL2 treatment, we found a dramatic increase in lung and liver metastases and an increase in CTC numbers (Fig. 1b–d and Extended Data Fig. 4a, b). Thus, although anti-CCL2 treatment reduced metastases, interruption of the treatment aggravated metastasis when compared to controls. However, the anti-metastatic effect persisted when animals were treated continuously with anti-CCL2 antibody (Extended Data Fig. 4c, d).

Since Ly6C-positive monocytes respond to CCL2, we assessed this paradoxical effect of CCL2 by focusing on the chemoattraction between breast cancer cells and $SSC^{low}CD11b^+Ly6C^+$ monocytes. We found that CCL2 drives mutual attraction of monocytes and tumour cells in vitro (Extended Data Fig. 5a–c). Monocytes were sequestered in the bone marrow during anti-CCL2 treatment (Extended Data Fig. 6a, b, left).
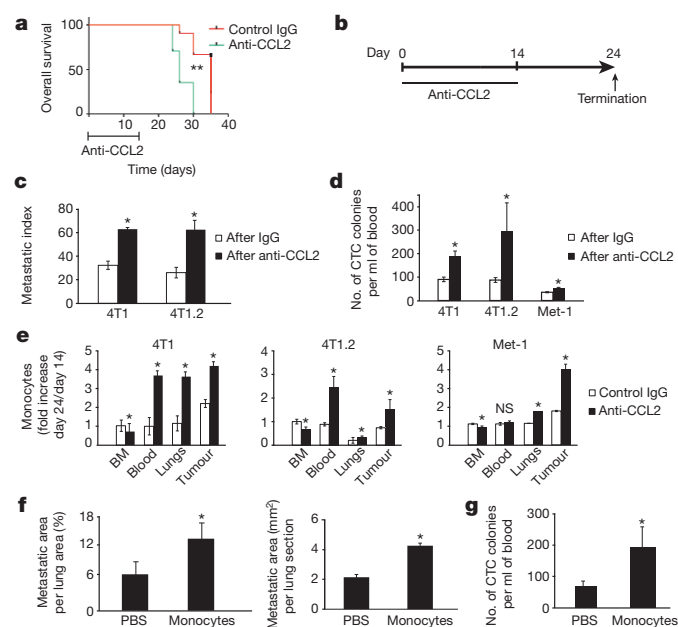

Figure 1 | Discontinuation of anti-CCL2 treatment increases lung metastases and accelerates death of mice. a, Kaplan–Meier survival curves of mice treated with anti-CCL2 antibody or control IgG for 14 days. The primary tumour was removed on the last day of treatment and the animals were left untreated until first signs of distress. $n = 12$ mice per group (pooled data of two experiments); black box, one animal was censored. **$P = 0.0001$, log-rank test. **b,** Timeline of the in vivo experiments. **c,** Metastatic index in tumour-bearing mice on day 24. **d,** Number of colonies formed by CTCs per ml blood on day 24. **e,** Ratio of $SSC^{low}CD11b^+Ly6C^+$ monocytes in organs on day 24 and on the last day of treatment (day 14). BM, bone marrow. **f,** Lung metastases were quantified as percentage of metastatic area per lung area (left) or as area per lung section (right) on five random sections per animal. **g,** Number of colonies formed by CTCs per ml blood. **c–g,** Data are shown as means ± standard error of the mean (s.e.m.) of $n = 8$ mice per group, pooled data from two experiments. *$P < 0.05$, unpaired t-test. NS, not significant.

[1]Friedrich Miescher Institute for Biomedical Research (FMI), Basel 4058, Switzerland. [2]Novartis Institutes for Biomedical Research, 4002 Basel, Switzerland. [3]Department of Pathology, University Hospital Zurich, 8006 Zurich, Switzerland. [4]Institute of Pathology Liestal, Cantonal Hospital Basselland, 4410 Liestal, Switzerland. †Present address: Koch Institute for Integrative Cancer Research, Massachusetts Institute of Technology, Cambridge, Massachusetts 02139, USA.
*These authors contributed equally to this work.

Ten days after treatment, monocyte numbers decreased in the bone marrow of animals treated with anti-CCL2 but increased in the primary tumour and lungs (Fig. 1e and Extended Data Fig. 6a–c, right). Therefore, monocytes were retained in the bone marrow during anti-CCL2 treatment and were released after treatment.

To assess monocyte distribution in tumours and metastases during and after CCL2 neutralization, we transferred sorted monocytes from bone marrow of 4T1.2-tumour-bearing mice into syngeneic tumour-bearing mice that had been treated for 7 days with anti-CCL2 or control immunoglobulin (Ig)G. During anti-CCL2 treatment, the transferred monocytes were retained in the bloodstream and their homing to the primary tumour and to the metastatic site was inhibited (Extended Data Fig. 7a). By contrast, 7 days after anti-CCL2 treatment cessation, transferred monocytes migrated to the lungs (Extended Data Fig. 7b).

To assess whether migration of monocytes into the primary tumour and lungs drives metastasis, tumour-bearing animals were transfused with monocytes from syngeneic tumour-bearing donors for 4 consecutive days. This enhanced lung metastases and numbers of CTCs (Fig. 1f, g) compared with controls. The data show that monocytes homed from the blood to the primary tumour or to the lungs in a CCL2-dependent manner and thus increased CTCs and lung metastases.

We then asked whether monocytes mediate the metastatic overshoot after cessation of anti-CCL2 treatment via enhanced mobilization of cancer cells from the primary tumour or through direct promotion of metastatic growth in the lungs. We removed the primary tumour on the last day of anti-CCL2 treatment and assessed lung metastases 10 days later. Lung metastases were still increased even though CTCs were reduced (Extended Data Fig. 8a, b). Furthermore, the number of monocytes/macrophages within lung metastases roughly doubled but increased to a lesser extent in the metastases of controls (Extended Data Fig. 8c). This suggested that the growth-enhancing effect of monocytes in the lungs crucially contributed to metastatic overshoot. Indeed, monocytes augmented the proliferation of breast cancer cells *in vitro* (Extended Data Fig. 8d). Since this direct effect was only moderate, we surmised that monocytes may also affect metastatic growth through effects on the metastatic microenvironment. We detected increased intrametastatic vasculature and Ki67$^+$ proliferating cells in metastases after anti-CCL2 discontinuation (Fig. 2a, b). Therefore, the enhancement of metastasis by monocytes could be due to a growth-enhancing effect of monocytes on tumour cells and to increased vascularization of metastases. To further test this hypothesis, we treated mice with anti-CCL2 or IgG for 14 days, followed by colony stimulating factor 1 receptor (CSF1R) inhibitor or vehicle (Fig. 2c). Since treatment with CSF1R inhibitor depletes CSF1R-positive cells[17] (Extended Data Fig. 8e), we concluded that monocyte depletion after anti-CCL2 treatment prevented metastatic overshoot (Fig. 2d). Vascular density and proliferation of metastases were also reduced (Fig. 2e, f and Extended Data Fig. 8e). High CCL2 in human breast cancer biopsies also correlated with high vascularization (Extended Data Fig. 9a) and with a high frequency of CD68$^+$ macrophages (Extended Data Fig. 1a). We conclude that an enhanced number of monocytes/macrophages in the lung after anti-CCL2 treatment cessation supports local vascular growth and proliferation of metastases.

To delineate the molecular mechanism by which monocytes increase vascular density within lung metastases after anti-CCL2 treatment, we analysed cytokines in supernatants of mono- and co-cultures of cancer cells and bone marrow monocytes. Among the cytokines that were increased in tumour–monocyte co-cultures compared with monocultures (Extended Data Fig. 9b, c), IL-6 was the only one known to stimulate angiogenesis[18,19]. Although IL-6 was not elevated in the primary tumour after anti-CCL2, its expression in serum and metastatic lungs was higher than in controls (Extended Data Fig. 9d and Fig. 3a). In addition, IL-6 induced expression of pro-angiogenic VEGF-A in monocytes *ex vivo*. This effect appeared to be CCL2 dependent (Fig. 3b). Consistently, analysis of gene expression data sets for metastatic breast cancer revealed that concomitant high expression of IL-6 in tumours with high CCL2 expression was associated with diminished patient survival, compared
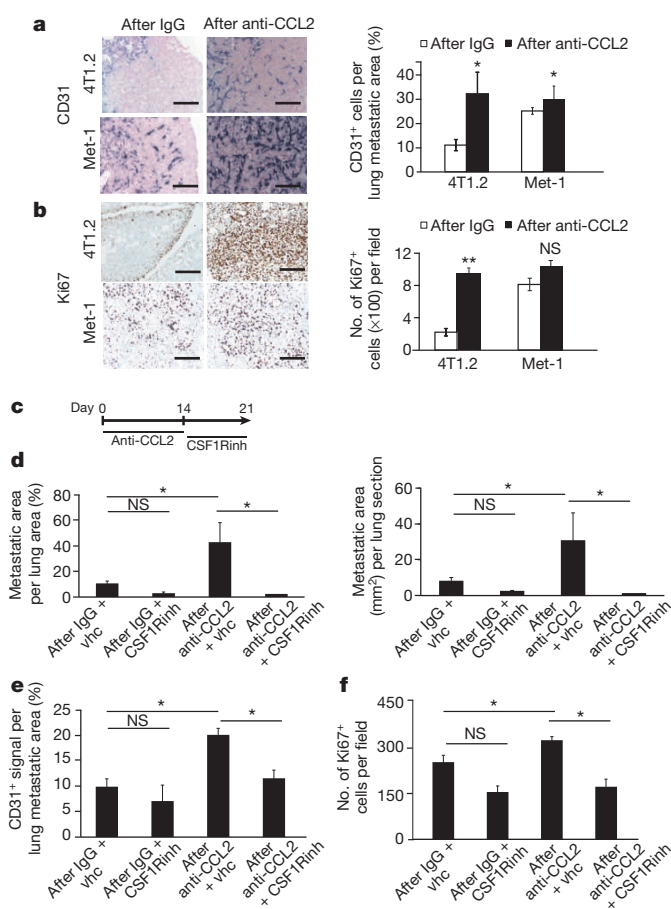

Figure 2 | Monocytes induce blood vessel formation and proliferation of lung metastases after discontinuation of anti-CCL2 treatment. a, Left, representative images of CD31-stained lung metastases on day 24. Scale bar, 50 μm. Right, quantification of CD31 staining. **b**, Left, representative images of Ki67-stained lung metastases on day 24. Scale bar, 100 μm. Right, quantification of Ki67 staining. **a, b**, Graphs show means ± s.e.m. of 20 fields of view on 5 lung sections per animal, $n = 4$ mice per group, pooled data from two experiments. **$P < 0.001$, *$P < 0.05$, unpaired t-test. One representative image out of 20 is shown per group. **c**, Timeline of *in vivo* experiments. CSF1Rinh, CSF1R inhibitor. **d**, Lung metastases were quantified as percentage of metastatic area per lung area (left) or as area per lung section (right). vhc, vehicle. **e**, Quantification of CD31 staining. **f**, Quantification of Ki67 staining. **d–f**, Graphs show means ± s.e.m. of 10 fields of view on 5 lung sections per animal, $n = 4$ mice per group, pooled data from two experiments. *$P < 0.05$, analysis of variance (ANOVA) with post-hoc Bonferroni correction. NS, not significant.

with concomitant low expression of IL-6 (Extended Data Fig. 9e). We conclude that high expression of IL-6 in the lungs subsequent to the cessation of anti-CCL2 treatment induces VEGF-A in monocytes and, at the same time, increases local vascular density.

Since IL-6 appeared to drive blood vessel density in metastatic lungs, we treated mice with anti-CCL2 followed by anti-IL-6. We observed reduced lung metastases and CTCs and increased survival of the mice (Fig. 3c, d and Extended Data Fig. 9f). We then asked whether anti-IL-6 decreased angiogenesis and tumour cell proliferation within metastases. Treatment of tumour-bearing animals with anti-IL-6 after anti-CCL2 reduced the overshooting number of CD31$^+$ cells in lungs and VEGF-A levels in lungs and serum (Fig. 3e, f and Extended Data Fig. 9g). Consistently, the proliferation of metastatic tumour cells declined to undetectable levels (Fig. 3g). Next we sought to understand how IL-6 induces VEGF-A expression *in vivo*. STAT3 phosphorylation (p-STAT3) results in VEGF-A secretion downstream of IL-6 signalling[20,21]. Therefore we assessed the level of p-STAT3 in lung metastatic tissue. Consistent with
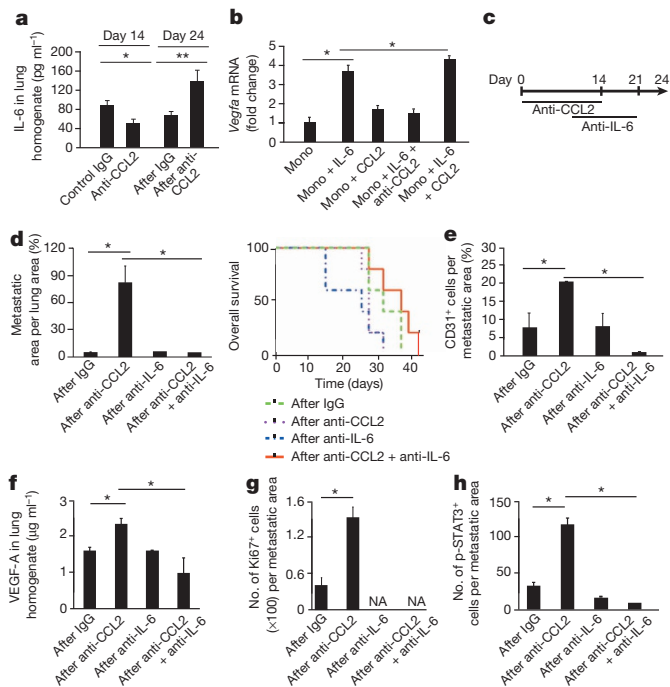
Figure 3 | Anti-IL-6 treatment after cessation of anti-CCL2 therapy prevents the overshoot of lung metastases. a, IL-6 expression in lung homogenates on day 14 and 10 days after anti-CCL2 treatment. Data are shown as means $\pm$ s.e.m., $n = 4$ mice per group, pooled data from two experiments. *$P < 0.05$, **$P < 0.001$, unpaired t-test. **b**, Mean *Vegfa* messenger RNA levels in monocytes (Mono) from tumour-bearing mice treated *ex vivo* with IL-6 and/or anti-CCL2. Data show means $\pm$ s.e.m., $n = 3$ mice per group, one representative of three independent experiments. *$P < 0.05$, ANOVA with post-hoc Bonferroni correction. **c**, Timeline of *in vivo* experiments. **d**, Left, quantification of lung metastases. Right, Kaplan–Meier survival curves of animals treated with control IgG, anti-CCL2, anti-IL-6 or anti-CCL2 plus anti-IL-6 as in Fig. 3c. On day 24, the animals were left without treatment until the appearance of signs of distress. $n = 10$ mice per group. $P = 0.0017$ by the log-rank test comparing anti-CCL2 with anti-CCL2 plus anti-IL-6 treatment. **e**, Quantification of CD31 staining. **f**, VEGF-A expression in lung homogenates from mice treated as in Fig. 3c measured by enzyme-linked immunosorbent assay (ELISA). Data are shown as means $\pm$ s.e.m., $n = 8$ mice per group, pooled data from two experiments. *$P < 0.05$, ANOVA with post-hoc Bonferroni correction. **g**, Quantification of Ki67 staining. **d** (left), **e**, **g**, Data show means $\pm$ s.e.m. of 20 fields of view on 5 sections per animal, $n = 4$ animals per group, pooled data from two experiments. *$P < 0.05$, ANOVA with post-hoc Bonferroni correction. NA, not applicable. **h**, Quantification of p-STAT3 staining. Data are shown as means $\pm$ s.e.m. of 10 fields of view on 5 sections per animal, $n = 4$ mice per group, pooled data from two experiments. *$P < 0.05$, ANOVA with post-hoc Bonferroni correction.

the increases in IL-6 and VEGF-A in the lungs, p-STAT3 also increased upon discontinuation of anti-CCL2 (Fig. 3h). These results suggest that IL-6/p-STAT3 pro-angiogenic effects contributed to the metastatic overshoot after cessation of anti-CCL2 treatment.

We neutralized VEGF-A *in vivo* to assess whether it supported tumour cell proliferation after anti-CCL2 or IgG treatment (Fig. 4a). This prevented metastatic overshoot, reduced blood-vessel density and reduced proliferation in lung metastases (Fig. 4b, c). p-STAT3 levels in the lungs did not change with this treatment (Extended Data Fig. 10a), suggesting that VEGF-A acts downstream of p-STAT3.

To confirm that monocytes/macrophages contributed to the expression of VEGF-A after cessation of anti-CCL2, we assessed p-STAT3 and VEGF-A levels in lungs from animals treated with anti-CCL2 or IgG control, followed by macrophage depletion with CSF1R inhibitor. p-STAT3 and VEGF-A levels increased in lungs of animals after cessation of anti-CCL2 treatment, but not if anti-CCL2 treatment was followed by monocyte/macrophage depletion (Fig. 4d, e and Extended Data Fig. 10b).
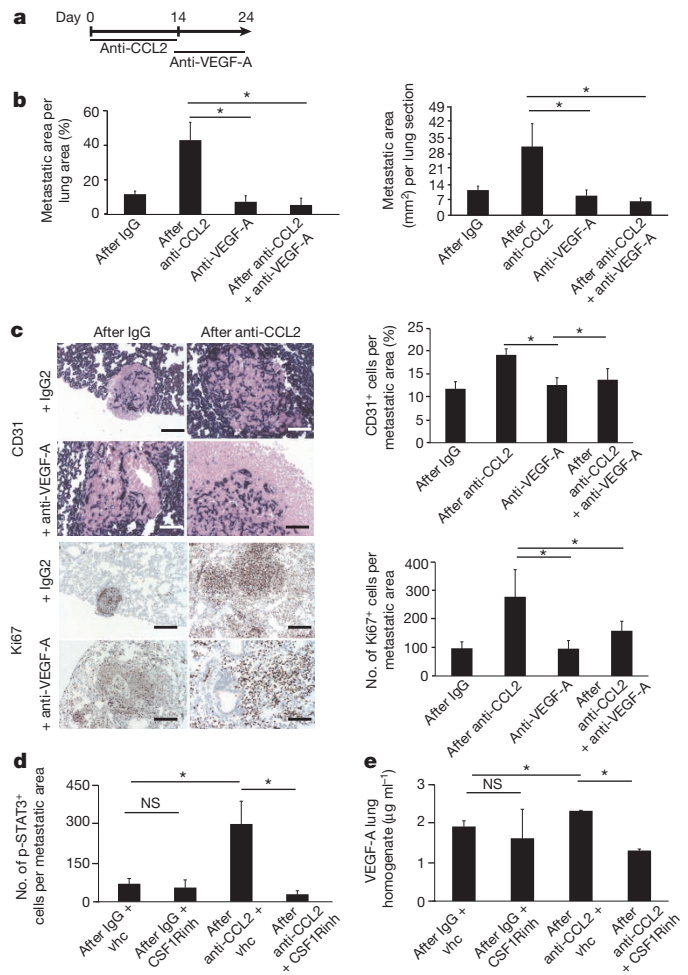

Figure 4 | Combined anti-CCL2 and anti-VEGF treatment reduces angiogenesis and tumour cell proliferation in lung metastases. a, Timeline of the *in vivo* experiments. **b**, Quantification of lung metastases as percentage of metastatic area per lung area (left) or as area per lung section (right). Data are shown as means $\pm$ s.e.m. of 20 fields of view on 5 lungs sections per animal, $n = 8$ mice per group, pooled data from two experiments. *$P < 0.05$, ANOVA with post-hoc Bonferroni correction. **c**, Top left, representative images of CD31-stained lungs on day 24. Top right, quantification of CD31 staining. Data are shown as means $\pm$ s.e.m. of 20 fields of view on 5 lung sections per animal, $n = 4$ mice per group, pooled data from two experiments. *$P < 0.05$, ANOVA with post-hoc Bonferroni correction. Scale bar, 100 μm. Bottom left, representative images of Ki67-stained lung on day 24. Bottom right, quantification of Ki67 staining. Data are shown as means $\pm$ s.e.m. of 20 fields of view on 5 lung sections per animal, $n = 3$ mice per group, pooled data from two experiments. *$P < 0.05$, ANOVA with post-hoc Bonferroni correction. Scale bar, 100 μm. One representative image out of 20 is shown per group. **d**, Quantification of p-STAT3 staining. Data are shown as means $\pm$ s.e.m. of 10 fields of view on 5 sections per animal, $n = 3$ mice per group, pooled data from two experiments. *$P < 0.05$, ANOVA with post-hoc Bonferroni correction. CSF1Rinh, CSF1R inhibitor; vhc, vehicle. **e**, VEGF-A expression in lung homogenates from mice treated as in Fig. 4a measured by ELISA. Data are shown as means $\pm$ s.e.m., $n = 3$ mice per group, pooled data from two experiments. *$P < 0.05$, ANOVA with post-hoc Bonferroni correction. NS, not significant.

This suggested that IL-6/p-STAT3-dependent VEGF-A secretion in the lung after cessation of CCL2 neutralization is indeed mediated by lung macrophages.

Together, these data support the idea that the complex tumour microenvironment is critical for effective anti-tumour strategies. Anti-CCL2 treatment decreased breast cancer metastases in mice, but interruption of anti-CCL2 treatment precipitated an unexpected influx of monocytes into the metastatic site and overshooting IL-6 levels within the

metastatic microenvironment. This led to local enhancement of angiogenesis, metastatic disease and a fatal outcome. Therefore our results prompt extreme caution when considering anti-CCL2 treatment of metastatic breast cancer and other neoplasias and suggest that therapeutic interference with the tumour microenvironment might lead to tissue remodelling not only locally but also at remote sites such as the bone marrow, with unexpected far-reaching consequences including a worsened prognosis for cancer patients. Any tumour immunotherapy that only sequesters immune cells away from the tumour and that does not permanently reprogram the tissue microenvironment or directly kill tumour cells may bear a similar risk of lethal rebound.

Online Content Methods, along with any additional Extended Data display items and Source Data, are available in the online version of the paper; references unique to these sections appear only in the online paper.

1. Qian, B. Z. et al. CCL2 recruits inflammatory monocytes to facilitate breast-tumour metastasis. *Nature* **475,** 222–225 (2011).
2. Lu, X. & Kang, Y. Chemokine (C-C motif) ligand 2 engages CCR2$^+$ stromal cells of monocytic origin to promote breast cancer metastasis to lung and bone. *J. Biol. Chem.* **284,** 29087–29096 (2009).
3. Wolf, M. J. et al. Endothelial CCR2 signaling induced by colon carcinoma cells enables extravasation via the JAK2-Stat5 and p38MAPK pathway. *Cancer Cell* **22,** 91–105 (2012).
4. Pietras, K. & Ostman, A. Hallmarks of cancer: interactions with the tumor stroma. *Exp. Cell Res.* **316,** 1324–1331 (2010).
5. McAllister, S. S. & Weinberg, R. A. Tumor-host interactions: a far-reaching relationship. *J. Clin. Oncol.* **28,** 4022–4028 (2010).
6. Hanahan, D. & Coussens, L. M. Accessories to the crime: functions of cells recruited to the tumor microenvironment. *Cancer Cell* **21,** 309–322 (2012).
7. Karnoub, A. E. & Weinberg, R. A. Chemokine networks and breast cancer metastasis. *Breast Dis.* **26,** 75–85 (2007).
8. Kleer, C. G., van Golen, K. L. & Merajver, S. D. Molecular biology of breast cancer metastasis. Inflammatory breast cancer: clinical syndrome and molecular determinants. *Breast Cancer Res.* **2,** 423–429 (2000).
9. Palangie, T. et al. Prognostic factors in inflammatory breast cancer and therapeutic implications. *Eur. J. Cancer* **30,** 921–927 (1994).
10. Ueno, T. et al. Significance of macrophage chemoattractant protein-1 in macrophage recruitment, angiogenesis, and survival in human breast cancer. *Clin. Cancer Res.* **6,** 3282–3289 (2000).
11. Valković, T., Lucin, K., Krstulja, M., Dobi-Babic, R. & Jonjic, N. Expression of monocyte chemotactic protein-1 in human invasive ductal breast cancer. *Pathol. Res. Pract.* **194,** 335–340 (1998).
12. Saji, H. et al. Significant correlation of monocyte chemoattractant protein-1 expression with neovascularization and progression of breast carcinoma. *Cancer* **92,** 1085–1091 (2001).
13. Chavey, C. et al. Oestrogen receptor negative breast cancers exhibit high cytokine content. *Breast Cancer Res.* **9,** R15 (2007).
14. Goede, V., Brogelli, L., Ziche, M. & Augustin, H. G. Induction of inflammatory angiogenesis by monocyte chemoattractant protein-1. *Int. J. Cancer* **82,** 765–770 (1999).
15. Li, X. et al. A destructive cascade mediated by CCL2 facilitates prostate cancer growth in bone. *Cancer Res.* **69,** 1685–1692 (2009).
16. Bonapace, L. et al. If you don't look, you won't see: intravital multiphoton imaging of primary and metastatic breast cancer. *J. Mammary Gland Biol. Neoplasia* **17,** 125–129 (2012).
17. Strachan, D. C. et al. CSF1R inhibition delays cervical and mammary tumor growth in murine models by attenuating the turnover of tumor-associated macrophages and enhancing infiltration by CD8 T cells. *OncoImmunology* **2,** e26968 (2013).
18. Nilsson, M. B., Langley, R. R. & Fidler, I. J. Interleukin-6, secreted by human ovarian carcinoma cells, is a potent proangiogenic cytokine. *Cancer Res.* **65,** 10794–10800 (2005).
19. Wani, A. A., Jafarnejad, S. M., Zhou, J. & Li, G. Integrin-linked kinase regulates melanoma angiogenesis by activating NF-κB/interleukin-6 signaling pathway. *Oncogene* **30,** 2778–2788 (2011).
20. Wei, D. et al. Stat3 activation regulates the expression of vascular endothelial growth factor and human pancreatic cancer angiogenesis and metastasis. *Oncogene* **22,** 319–329 (2003).
21. Wei, L. H. et al. Interleukin-6 promotes cervical tumor growth by VEGF-dependent angiogenesis via a STAT3 pathway. *Oncogene* **22,** 1517–1527 (2003).

Supplementary Information is available in the online version of the paper.

Author Contributions L.B., M.-M.C., T.J. and M.B.-A. designed and performed most of the experiments and wrote the manuscript. K.D.M. and Z.V. performed human biopsy experiments. J.W., M.-M.C. and L.B. performed intravital imaging. All authors prepared the manuscript.

METHODS

Patient cohorts. Samples from paraffin-embedded invasive breast cancer tissues ($n = 30$) were retrieved from the archives of the Institute of Surgical Pathology, University Hospital Zurich and the Institute of Pathology, Cantonal Hospital Baselland, Liestal, Switzerland. The minimum follow-up time was 2 years. Clinico-pathological data for all patients were available. All biopsies were collected for previous diagnostic purposes and processed according to standard procedures. Two board-certified pathologists (K.D.M., Z.V.) verified the diagnoses of invasive breast carcinoma.

The retrospective study on formalin-fixed, paraffin-embedded human breast cancer tissue was approved by the Cantonal Ethical Committee of Zurich (KEK-2012-553). Informed consent was not necessary, as the ethical approval covered the ethical issues of the retrospective study and the samples were completely anonymized and de-identified before the study. For immunohistochemical studies, two groups of breast cancer patients were examined: Group 1 ($n = 14$; 12 hormone-receptor positive, 2 triple negative) were primary breast cancer patients without lymph node or distal metastases; Group 2 patients ($n = 16$; 14 hormone-receptor positive, 2 triple negative) had both lymph node involvement and distant metastases, except for three patients with lymph node metastases whose distant metastasis status was unknown at the time of this study.

Immunohistochemistry. For all cases, three sequential whole-tissue sections were stained with the antibodies anti-CD68 (DAKO-Cytomation, clone PG-M1, 1:100 dilution), anti-CD31 (Novocastra, clone 1A10, 1:100 dilution, Leica Biosystems) and anti-CCL2 (R&D Systems, clone 23002, 1:100 dilution). Immunohistochemistry on 4-μm sections was performed using an automated immunohistochemistry Bond platform (Leica Biosystems). Detection was carried out with Refine-Red or Refine-DAB kits (Bond), including the respective secondary antibodies. The sections were visualized with an Olympus BX41 microscope and attached Olympus UC30 camera using the cell^A digital imaging acquisition software (Olympus).

The number of CD68-positive macrophages per high-power field (HPF) was counted automatically. CD68-positive elements were only counted as macrophages if a nucleus could be identified in the section and only intratumoral macrophages were taken into account. The mean of 20 HPFs was calculated for each case. Similarly, the number of CD31-positive vessels per HPF was counted automatically (20 HPFs per case). Only areas of positive staining with a minimal diameter of 20 μm were taken into account to exclude isolated CD31$^+$ cells. Cytoplasmic CCL2 staining within tumour cells was scored manually by a board-certified pathologist (K.D.M.) according to a three-tiered system: 0 (negative staining, no detectable staining), 1+ (staining in <10% of tumour cells), 2+ (staining in >10% of tumour cells).

Tumours grown in mice were fixed in 10% neutral buffered formalin (NBF) for 24 h at 4 °C, washed with 70% ethanol, embedded in paraffin, sectioned at 3 μm, and stained with haematoxylin and eosin (H&E), anti-Ki67 (clone PA5-19462, 1:400 dilution, Thermo Scientific) or anti-CD31 (clone 390, 1:500 dilution, Invitrogen) antibodies. The investigator was blinded in all the immunohistochemistry quantifications.

Analysis of public microarray data. The publicly available processed data sets from The Cancer Genome Atlas (TCGA) for breast invasive carcinoma (AgilentG4502A_version 2013-07-12) were downloaded from https://genome-cancer.ucsc.edu/ and analysed with R/bioconductor[22-25]. Patients (all clinical subtypes) were split according to their CCL2 and IL-6 expression and the highest tertile were compared to the lowest tertile for each gene. The resulting groups were tested for difference in overall survival using the survival package in R by fitting a Cox proportional hazard regression model.

Reagents, recombinant proteins and antibodies. Recombinant mouse JE/MCP-1 (CCL2) and mouse IL-6 were purchased from Peprotech (Switzerland). Rat anti-mouse-IL-6 (clone MAB-406) and rat IgG1 control were from R&D Systems (UK). Purified NA/LE hamster anti-mouse MCP-1/CCL2 (clone 2H5) and hamster IgG2a control were purchased from BD Bioscience (Switzerland). Goat anti-mouse VEGF-A (clone AF493NA) and polyclonal goat IgG (R&D systems) were used for cell culture (1 μg ml^{-1}) and for in vivo experiments. CSF1R inhibitor was provided by D. Dylan[17].

The following anti-mouse antibodies were used for flow cytometry: CD11b (anti-mouse APC-CD11b, clone M1/70), Ly6C (anti-mouse FITC-Ly6C, clone HK1.4), Ly6G (anti-mouse Percp-Cy5.5-Ly6G, clone IA8), CD206 (anti-mouse FITC-CD206, clone C068C2), I-A/I-E (anti-mouse Percp-Cy5.5-I-A/I-E, clone M5/114.15.2), CD11c (anti-mouse Percp-Cy5.5-CD11c, clone N418), CD86 (anti-mouse Alexa-fluor 488 CD86, clone GL-1), all from BD Bioscience, and mCCR2 (anti-mouse FITC-CCR2), from R&D Systems.

Cell culture. Syngeneic mammary cancer 4T1 cells[26], 4T1.2 cells (derived from Balb/c mice, from R. L. Anderson), J110 cells (derived from FVB mice, from N. Hynes) and Met-1 cells (from FVB mice, from R. Cardiff) were cultured in DMEM supplemented with 10% FCS. In co-culture experiments, 10^5 tumour cells were incubated with 10^5 sorted primary bone marrow monocytes in DMEM 0.5% FCS. Cell viability was measured using a Neubauer chamber and trypan blue.

ELISA and cytokine arrays. CCL2 levels were assessed using the mCCL2 ELISA Duo-Set (R&D Systems) for mouse cells and the hCCL2 ELISA Duo-Set (R&D Systems) for human cells. IL-6 was measured by mIL-6 ELISA Duo-Set (R&D Systems). VEGF-A levels were assessed using the mVEGF-A Duo-set (R&D System). Cytokine arrays from R&D Systems were used according to the manufacturer's protocol.

Flow cytometry. Cultured adherent cells were detached using trypsin-EDTA, suspended in growth medium and counted. Tumours, lungs and bone marrow were mechanically and enzymatically dissociated (using collagenase II, Sigma). Cells were incubated with 2.5 μg antibodies per 10^6 cells or with 2.5 μg mouse IgG isotype control antibody (R&D Systems) per 10^6 cells for 20 min at 4 °C in the dark before washing and analysis. At least 10^4 cells per sample were analysed with a FACScalibur flow cytometer (Becton Dickinson). Monocytes were identified for quantification and sorting as SSC^{low}CD11b$^+$Ly6C$^+$ cells. The reference population for gating was SSC^{low}CD11b$^+$, thereby excluding granulocytes, as shown in Extended Data Fig. 5a. Absolute monocyte numbers were quantified as previously described[27]. In brief, after organ harvest, single-cell suspensions were obtained from bone marrow, blood, lung, or tumour. Total viable cell numbers were determined using Trypan Blue. Absolute monocyte numbers were calculated as number of total viable cells multiplied by the percentage of SSC^{low}CD11b$^+$Ly6C$^+$Gr1$^+$ monocytes of all live cells.

RNA and quantitative real-time PCR. Total RNA was extracted using the Trizol reagent according to the manufacturer's protocol (Ambion RNA, Life Technologies). Aliquots of 1 μg of total RNA were transcribed using the SuperScript III First-strand synthesis for RT–PCR (Invitrogen). PCR and fluorescence detection were performed using the StepOnePlus Sequence Detection System (Applied Biosystems) according to the manufacturer's protocol in a reaction volume of 20 μl containing 1× TaqMan Universal PCR Master Mix (Applied Biosystems) and 30 ng cDNA. For quantification of mouse *Ccl2*, *Hprt1*, *Vegfa* and *Il6* mRNA, the 1× TaqMan Gene Expression Assays Mm_00441242_m1, Mm00446968_m1, Mm01281449_m1 and Mm00446190_m1 (Applied Biosystems) were used. All measurements were performed in duplicates and the arithmetic means of the cycle threshold (Ct) values were used for calculations: target gene mean Ct values were normalized to the respective housekeeping gene (*Hprt1*), mean Ct values (internal reference gene, Ct), and then to the experimental control. The values obtained were exponentiated 2($-\Delta\Delta$Ct) to be expressed as n-fold changes in regulation compared with the experimental control (2($-\Delta\Delta$Ct) by the method of relative quantification[25].

Animal experiments. Experiments using FVB and Balb/c (Charles River Laboratory and Jackson Laboratory, respectively) mice were carried out according to Swiss national guidelines on animal welfare and the regulations of the Canton of Basel Stadt.

To induce spontaneous metastasis, $1–4 \times 10^6$ tumour cells of different lines were injected into the fourth mammary fat pad of 7- to 8-week-old female FVB or Balb/c mice. Antibody treatments were performed 3–15 days after tumour cell injection (depending on the cell line used) via intraperitoneal injection 3 times per week. Anti-CCL2, anti-IL6 and anti-VEGF antibodies or the respective controls were used at 1 mg kg^{-1}. The CFS1R inhibitor (200 mg kg^{-1} oral dosing) and the corresponding vehicle were administered daily.

Tumour volume was calculated using the formula: length × width^2/2. To assess the number of CTCs, blood was taken from the right atrium, plated in DMEM medium supplemented with 10% FCS, and colonies counted on day 10 of culture. The number of CTCs was calculated as the total number of colonies in the dish divided by the volume of blood taken. To quantify metastases, the lungs were fixed in Bouin's solution (Sigma Aldrich) for macrometastases or in PFA 4% for micrometastases.

For adoptive transfer of monocytes, tumour-bearing animals were killed on day 14 after orthotopic injection of cancer cell lines. SSC^{low}CD11b$^+$Ly6C$^+$ monocytes were sorted from femoral bone marrow into PBS and 1% FCS, stained with the vital dye CMTMR (5-(and-6)-(((4-chloromethyl)benzoyl)amino)tetramethylrhodamine; Invitrogen) for 10 min at 37 °C according to the manufacturer's protocol. Aliquots of 8×10^6 labelled cells were injected into the tail vein of syngeneic tumour-bearing mice that were treated with anti-CCL2 or the IgG control by intraperitoneal injection of fresh antibodies diluted in PBS (10 mg kg^{-1}). Mice were killed 1 day later and single-cell suspensions of the lungs, blood, bone marrow and primary tumours were counterstained with CD11b-APC and analysed by flow cytometry. To assess the effect of monocytes on metastases, 1×10^6 sorted SSC^{low}CD11b$^+$Ly6C$^+$ cells from tumour-bearing animals were injected into the tail vein of recipient syngeneic tumour-bearing animals daily for 4 consecutive days. The mice were killed on day 11 after tumour cell injection and CTCs and metastases were assessed as described earlier.

Intravital imaging. Orthotopic mammary tumours were grown for 1–2 weeks. Mice were anaesthetized with Attane Isofluran (Provet AG) and mounted on a custom-made stage. Anaesthesia was maintained throughout the experiment with a nose cone. Tumours were exposed by skin flap surgery[28] on a custom-made multiphoton microscope[16] and imaged at 880 nm with a ×25/1.05NA water immersion objective (Olympus) at a resolution of 1.06 μm per pixel. Cell motility was observed by time-lapse imaging over 30 min in 2-min cycles, where a 100 μm z-stack at

5-μm increments was recorded for each frame starting at the tumour capsule. Three-dimensional time-lapse videos were analysed using Image J[29]. Tumour cell motility was quantified manually. A tumour cell motility event was defined as a protrusion of half a cell length or more over the course of a 30 min video. For visualizing vasculature, 100 μl of 20 mg ml^{-1} 70 kDa Texas Red–dextran (Invitrogen, Molecular Probes) was injected into the tail vein of the mice before surgery and imaging of blood vessels and macrophages. Vasculature was quantified manually as tubes of at least 20 μm length appearing in the red channel. Permeability of the blood vessels was measured as the time taken by dextran to leak out from the blood vessels as reported previously[30].

Cell invasion. Invasion assays were performed using transwell chambers (8 μm pore size, BD Biocoat Growth factor-reduced Matrigel Invasion Chamber) according to the manufacturer's protocol. An aliquot of 5×10^4 cells in 100 μl of DMEM 0.1% BSA was plated into the top chamber and DMEM 10% FBS alone or containing monocytes derived from bone marrow of animals bearing autologous tumours was placed in the bottom chamber. After a 24 h incubation at 37 °C and 5% CO_2, cells at the lower surface of the membrane were fixed with 3.7% paraformaldehyde, stained with 0.2% crystal violet, and washed with 1× PBS. The number of cells per field was quantified microscopically and total cell number was evaluated by trypan blue vital.

Statistical analysis. All the *in vitro* experiments were performed in biological and technical triplicates. The number of mice was calculated by performing power analysis using data from small pilot experiments. Values represent the means ± s.e.m. Depending on the type of experiment, data were tested using two-tailed Student's *t*-test, log-rank test, or one-way ANOVA with post-hoc Bonferroni correction. *$P < 0.05$ and **$P < 0.001$ were considered statistically significant.

Immunohistochemistry on human samples was analysed with R/bioconductor[22–25] using a one-way ANOVA (assuming that the data are normally distributed). The different box plots represent the first to the third quartile of the data. The thick line is the median, and the whiskers in the box plot extend to the minimal and maximal values, after outliers have been removed. Outliers were defined by default as all data points that are more than 1.5-fold the box length (the interquartile range) away from the median.

22. The Cancer Genome Atlas Network. Comprehensive molecular portraits of human breast tumours. *Nature* **490,** 61–70 (2012).
23. Zhu, J. *et al.* The UCSC Cancer Genomics Browser. *Nature Methods* **6,** 239–240 (2009).
24. Goldman, M. *et al.* The UCSC Cancer Genomics Browser: update 2013. *Nucleic Acids Res.* **41,** D949–D954 (2013).
25. Schmittgen, T. D. Real-time quantitative PCR. *Methods* **25,** 383–385 (2001).
26. Aslakson, C. J. & Miller, F. R. Selective events in the metastatic process defined by analysis of the sequential dissemination of subpopulations of a mouse mammary tumor. *Cancer Res.* **52,** 1399–1405 (1992).
27. Swirski, F. K. *et al.* Identification of splenic reservoir monocytes and their deployment to inflammatory sites. *Science* **325,** 612–616 (2009).
28. Wyckoff, J., Gligorijevic, B., Entenberg, D., Segall, J. & Condeelis, J. High-resolution multiphoton imaging of tumors *in vivo. Cold Spring Harb. Protoc.* **2011,** 1167–1184 (2011).
29. Abramoff, M. D., Magelhaes, P. J. & Ram, S. J. Image Processing with Image. *J. Biophotonics Intl* **11,** 36–42 (2004).
30. Egawa, G. *et al.* Intravital analysis of vascular permeability in mice using two-photon microscopy. *Sci. Rep.* **3,** 1932 (2013).

a

b

n1=200 (CCL2low)
n2=200 (CCL2high)

c

d

e
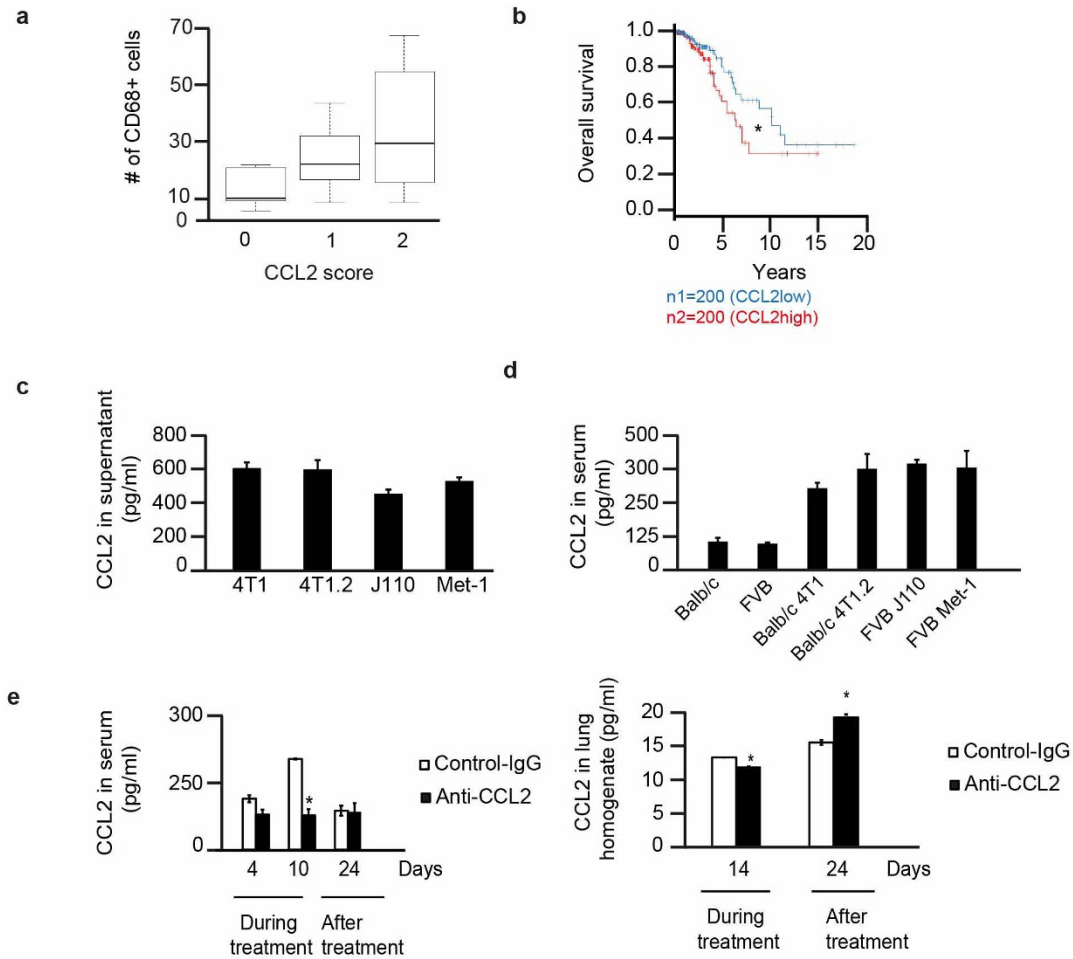
Extended Data Figure 1 | CCL2 is overexpressed in breast cancer. **a**, Positive correlation between immunohistochemical staining score of CCL2 and the number of CD68-positive macrophages per high-power field in human biopsies ($n = 30$). $P = 0.024$; data were analysed using R with one-way ANOVA (assuming that the data are normally distributed). The box plot represents the first to the third quartile of the data. Thick line indicates median, the whiskers extend to the minimal and maximal values. **b**, Kaplan–Meier survival curves showing overall survival of breast cancer patients with high or low CCL2 expression. $P = 0.0372$, log-rank test. **c**, CCL2 expression in supernatants of murine breast cancer cell lines grown *in vitro*. Data are shown as means ± s.e.m., $n = 3$ wells, one representative of three independent experiments. **d**, CCL2 expression in sera of mice bearing the indicated tumours for 14 days. Data are shown as means ± s.e.m., $n = 3$ animals per group, one representative of two independent experiments. **e**, CCL2 levels in sera (left) and lung homogenate (right) from 4T1.2-tumour-bearing mice during anti-CCL2 or IgG treatment or 10 days after the cessation of treatment. Data are shown as means ± s.e.m., $n = 5$ mice per group, pooled data from two independent experiments. *$P < 0.05$, unpaired *t*-test.
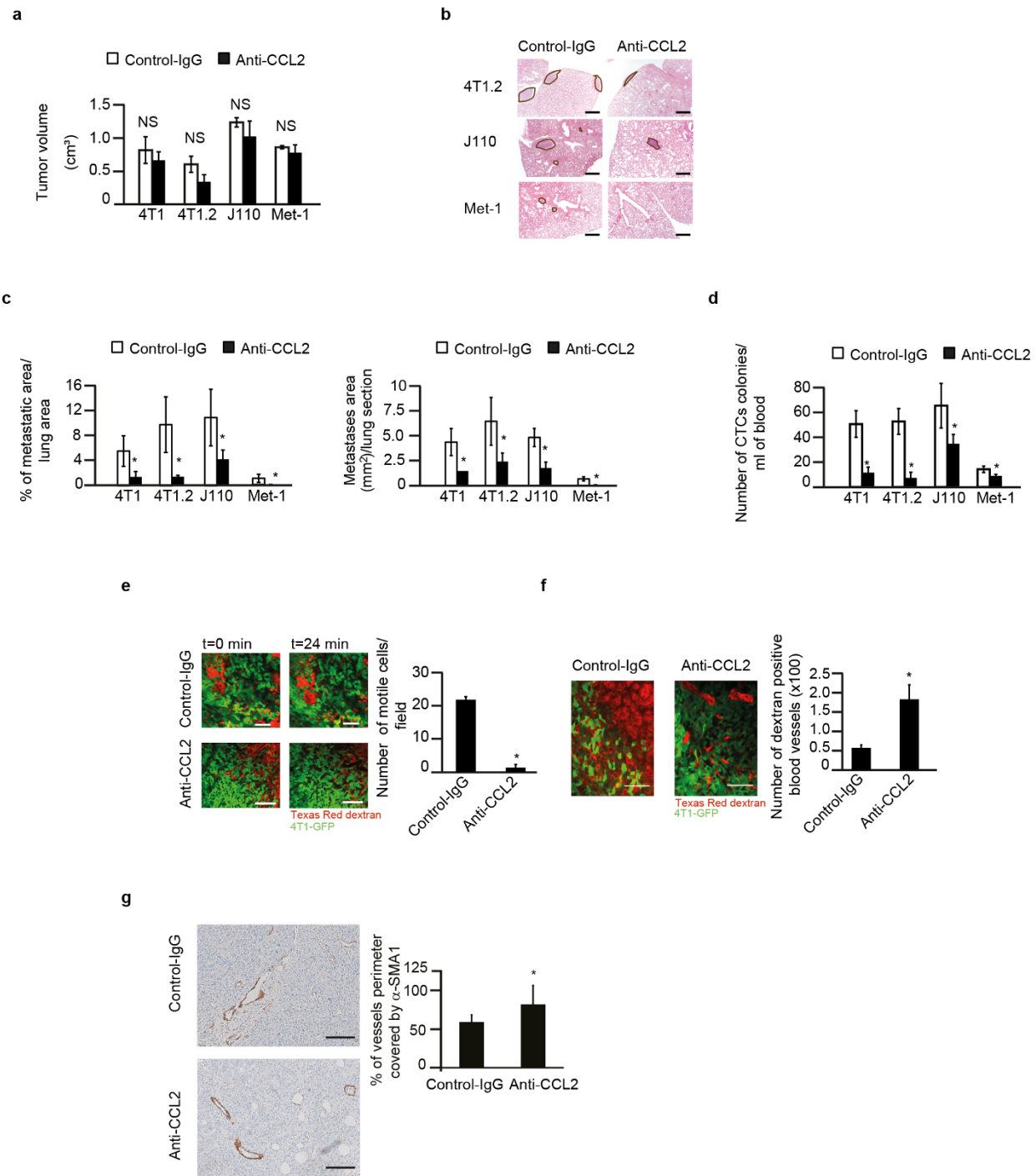
Extended Data Figure 2 | Anti-CCL2 treatment reduces breast cancer metastases. a, Tumour volumes on day 11 of treatment with anti-CCL2 or IgG. Data are shown as mean tumour volumes ± s.e.m., $n = 10$ mice, pooled data from two independent experiments. NS, not significant (unpaired t-test). **b**, Representative images of haematoxylin and eosin (H&E)-stained lung sections out of 20 images per group. Black circles indicate metastases. Scale bar, 500 μm. **c**, Quantification of metastases as percentage of metastatic area per lung area (left) or as metastatic area per lung section (right). Data are shown as means ± s.e.m. of 20 fields of view on 5 sections per animal, $n = 4$ mice per group, pooled data from two experiments. *$P < 0.05$, unpaired t-test. **d**, Effect of anti-CCL2 and IgG treatment on CTCs from tumour-bearing animals on day 11 of treatment. Data are shown as means ± s.e.m. of 20 fields of view on 5 sections per animal, $n = 4$ mice per group, pooled data from two experiments. *$P < 0.05$, unpaired t-test. **e**, Intravital multiphoton images of 4T1–GFP primary tumours on day 7 of treatment with anti-CCL2 antibody or IgG. Left, representative two-dimensional images out of 24 fields from primary tumours

(green) 50 μm below the tumour surface, 24 min after intravenous injection of 70 kDa Texas Red–dextran (red). Scale bar, 100 μm. Right, mean numbers of motile tumour cells ± s.e.m. per 30 min acquisition, 6 fields per mouse, $n = 4$ mice per group. *$P < 0.05$, unpaired t-test. **f**, Intravital multiphoton images of vasculature in 4T1–GFP primary tumours on day 7 of treatment. Left, representative two-dimensional images out of 12 fields per group, 50 μm below the tumour surface, 15 min after intravenous injection of 70 kDa Texas Red–dextran (red). Scale bar, 100 μm. Right, mean number of dextran-positive blood vessels counted over 42 min, starting 15 min after injection of Texas Red–dextran. Results are shown as means ± s.e.m., $n = 4$ mice per group and 3 fields per animal. *$P < 0.05$, unpaired t-test. **g**, Left, representative images out of 12 images per group from α-SMA1-stained 4T1.2 tumour sections. Scale bar, 500 μm. Right, quantification of the perimeter of blood vessels covered by α-SMA1 staining. Data are shown as percentage vessel perimeter covered by α-SMA1 ± s.e.m. of 12 fields of view on 4 sections per animal, $n = 3$ mice per group, pooled data from two experiments. *$P < 0.05$, unpaired t-test.
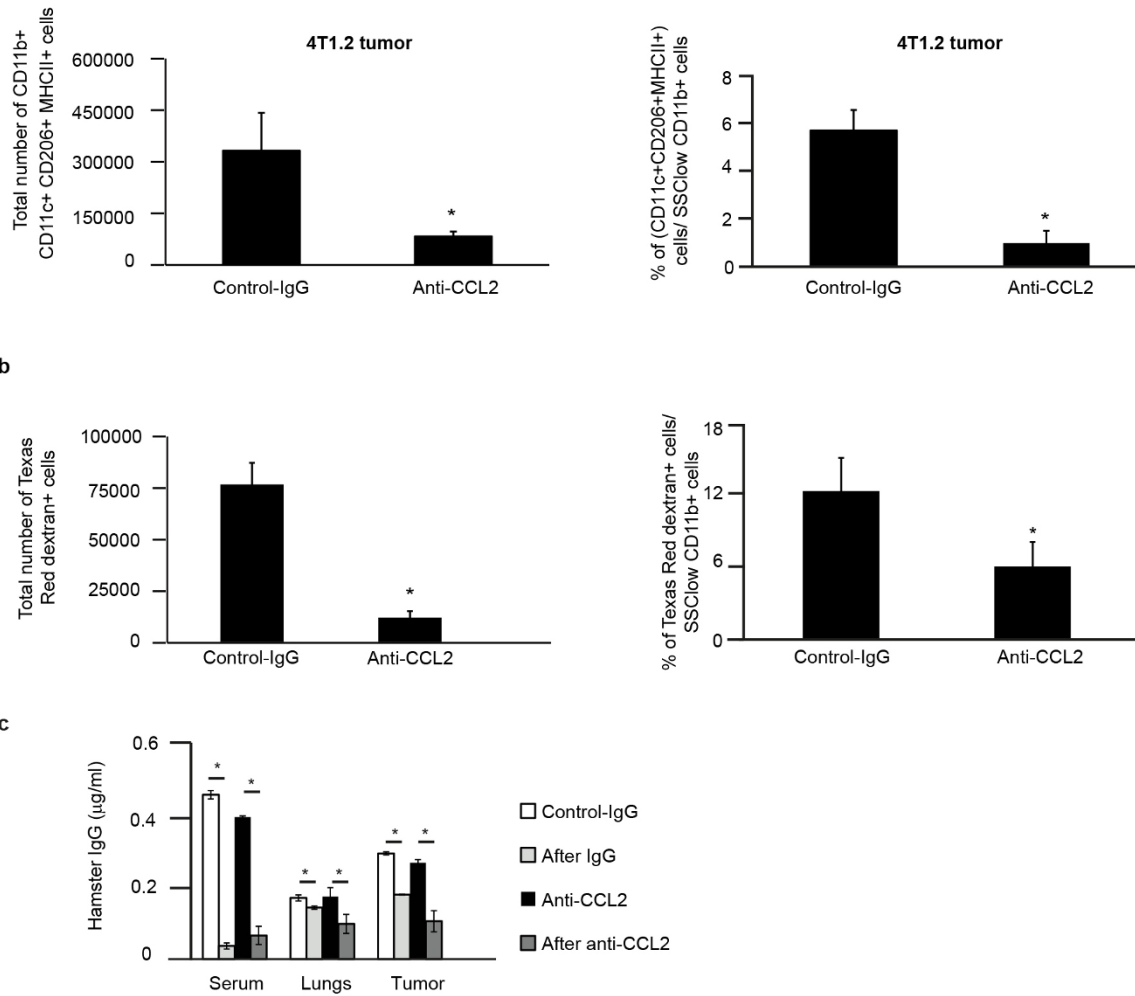
Extended Data Figure 3 | Macrophages decline in primary 4T1.2 tumours upon treatment with anti-CCL2. **a**, Left, total number of $SSC^{low}CD11b^{+}CD11c^{+}CD206^{+}MHCII^{+}$ macrophages. Right, percentage of $CD11c^{+}CD206^{+}MHCII^{+}$ macrophages per $SSC^{low}CD11b^{+}$ cell population. Data are shown as means ± s.e.m., $n = 3$ mice. *$P < 0.05$, unpaired t-test. **b**, Left, total number of Texas-Red-positive $SSC^{low}CD11b^{+}$ macrophages. Right, percentage of Texas-Red-positive macrophages per $SSC^{low}CD11b^{+}$ cells, enumerated by flow cytometry of 4T1.2 primary tumours from tumour-bearing mice treated for 14 days, after intravenous injection of Texas Red–dextran. Data are shown as means ± s.e.m., $n = 6$ mice pooled data of two independent experiments. *$P < 0.05$, unpaired t-test. **c**, Concentration of hamster IgG in serum, lung homogenates and tumour during treatment (day 14) and at 10 days after cessation of treatment as detected by ELISA. Data are shown as means ± s.e.m., $n = 4$ mice per group. *$P < 0.05$, **$P < 0.001$, unpaired t-test.

a
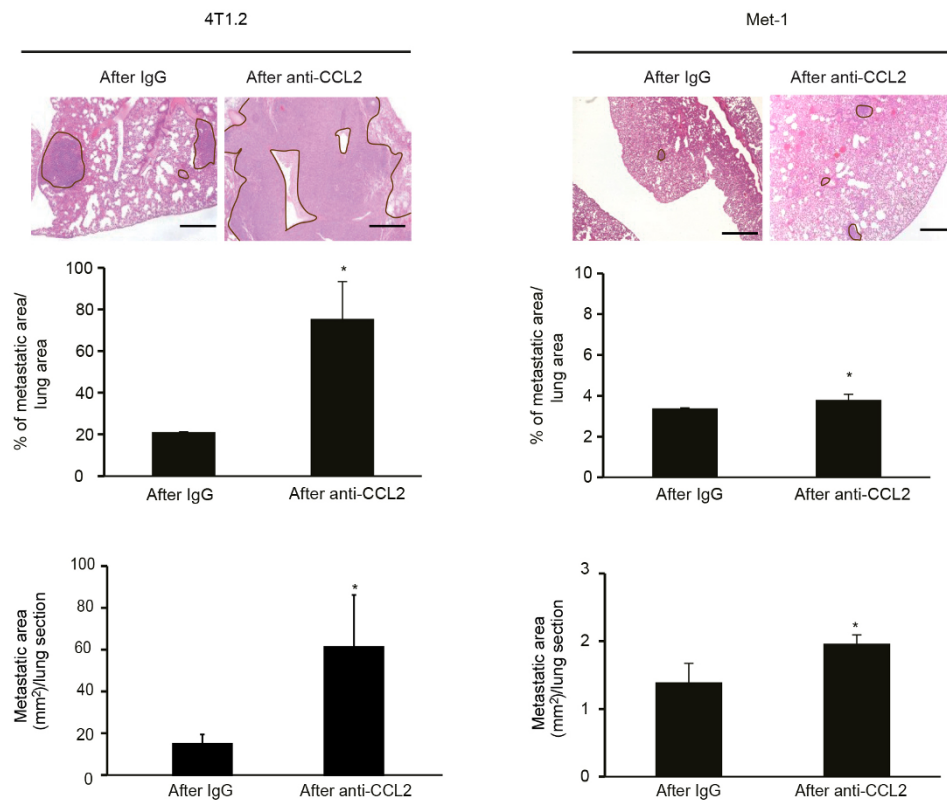
b
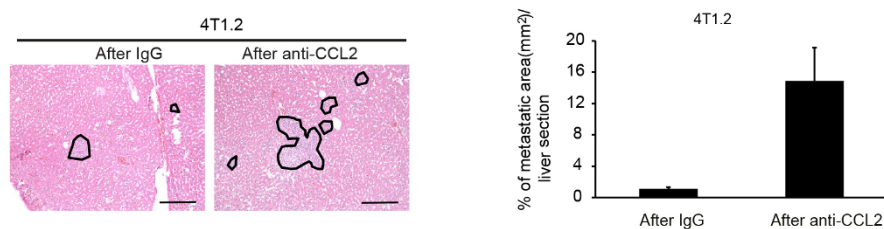
c

d
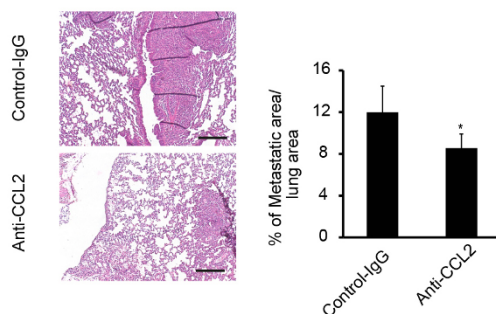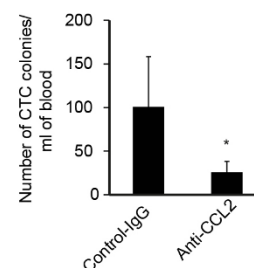
Extended Data Figure 4 | Cessation of anti-CCL2 treatment increases lung metastases. a, Top, representative H&E-stained lung sections from 4T1.2- and Met-1-tumour-bearing mice 10 days after cessation of treatment. Scale bar, 500 μm. Bottom, quantification of lung metastases as percentage of metastatic area per lung area and metastatic area per lung section. Data are shown as means ± s.e.m. of 20 fields of view on 5 sections per animal, $n = 4$ mice per group, pooled data from two experiments. *$P < 0.05$, unpaired t-test. One representative image out of 20 is shown per group. **b**, Left, representative H&E-stained liver sections from 4T1.2-tumour-bearing mice 10 days after cessation of treatment. Scale bar, 500 μm. Right, quantification of liver metastases as metastatic area per lung section. Data are shown as means ± s.e.m. of $n = 10$

fields of view on 5 sections per animal, $n = 2$ mice per group. *$P < 0.05$, unpaired t-test. One representative image out of 10 is shown per group. **c, d**, 4T1.2-tumour-bearing animals were treated for 24 consecutive days with anti-CCL2 or IgG control. **c**, Left, representative images of H&E-stained lung sections. Scale bar, 500 μm. Right, lung metastases were quantified as percentage of metastatic area per lung area on day 24 of treatment. Data are shown as means ± s.e.m. of 20 fields of view on 5 lungs sections per animal, $n = 4$ mice per group. *$P < 0.05$, unpaired t-test. One representative image out of 20 is shown per group. **d**, Number of colonies formed by CTCs per ml blood collected on day 24 of treatment. Data are shown as means ± s.e.m. of $n = 4$ mice per group. *$P < 0.05$, unpaired t-test.
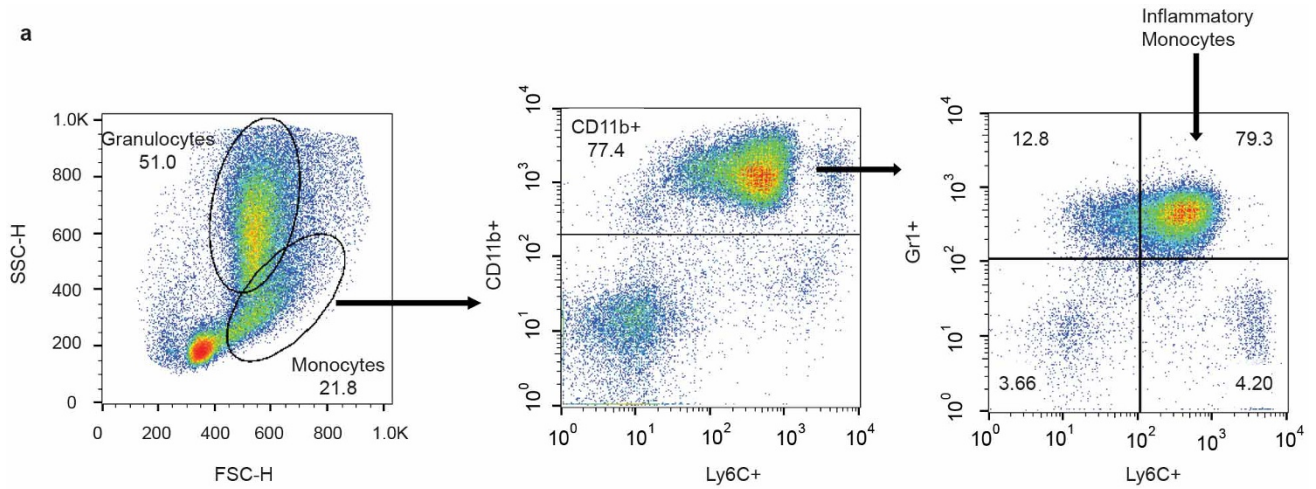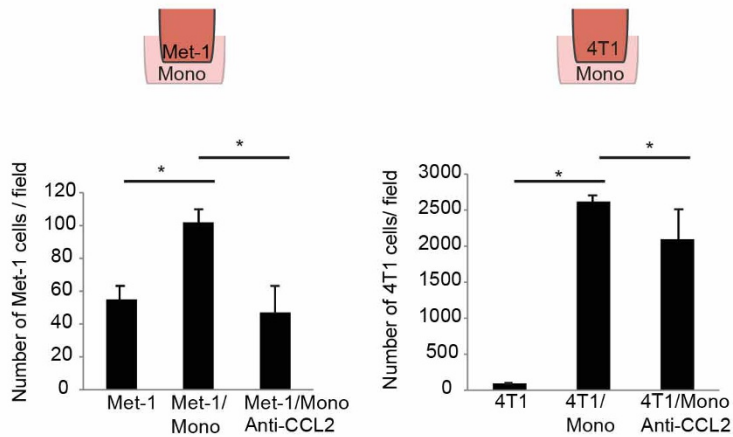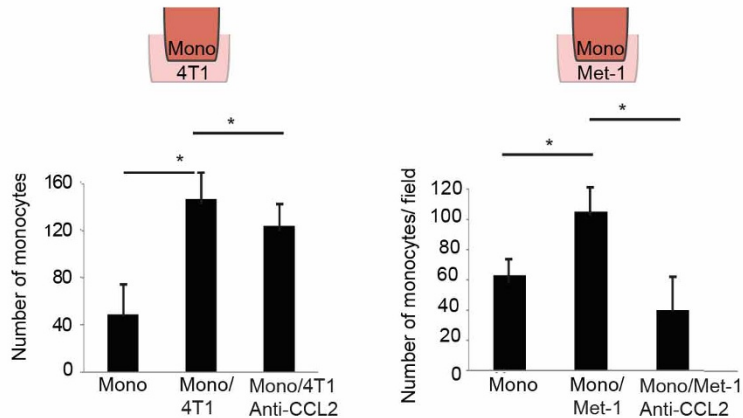
Extended Data Figure 5 | CCL2 drives mutual attraction of monocytes and tumour cells. a, Fluorescence-activated cell sorting (FACS) plots showing the gating strategy for identification and isolation of inflammatory monocytes. **b**, Transwell invasion assay of Met-1 cells (left) or 4T1 cells (right) on top of matrigel towards Ly6C$^+$ monocytes (Mono). Data are shown as means of invading cell numbers $\pm$ s.e.m., $n = 4$ independent experiments with each experiment performed in triplicate. *$P < 0.05$, ANOVA with Bonferroni post-test. **c**, Transwell invasion assay of Ly6C$^+$ monocytes on top of matrigel towards 4T1 (left) or Met-1 (right) cells. Data are shown as means of invading cell numbers $\pm$ s.e.m., $n = 3$ independent experiments with each experiment performed in triplicate. *$P < 0.05$, ANOVA with post-hoc Bonferroni correction.
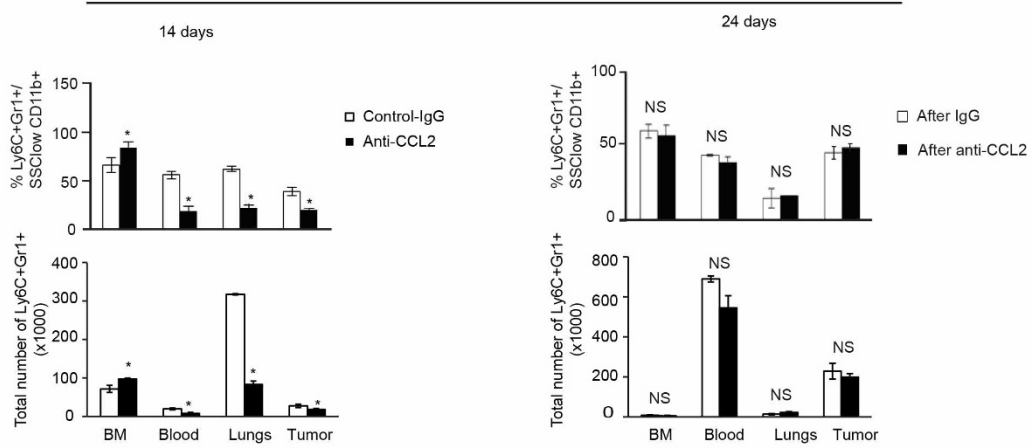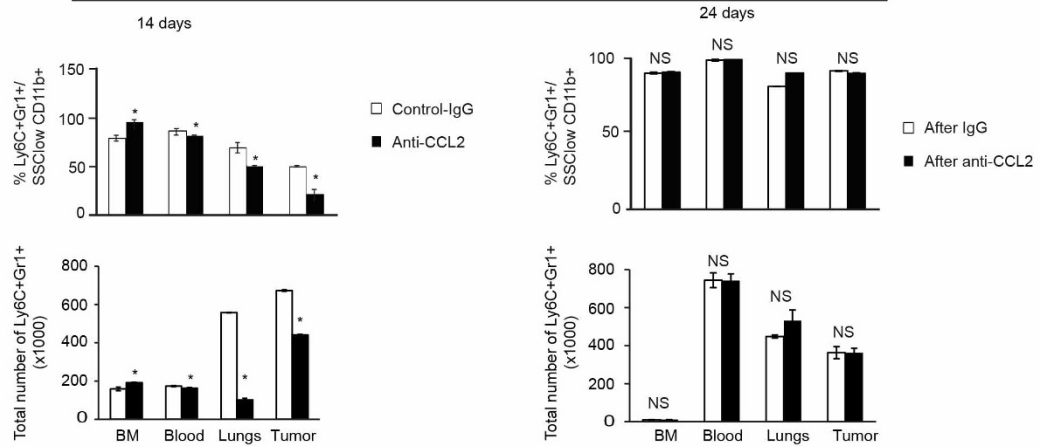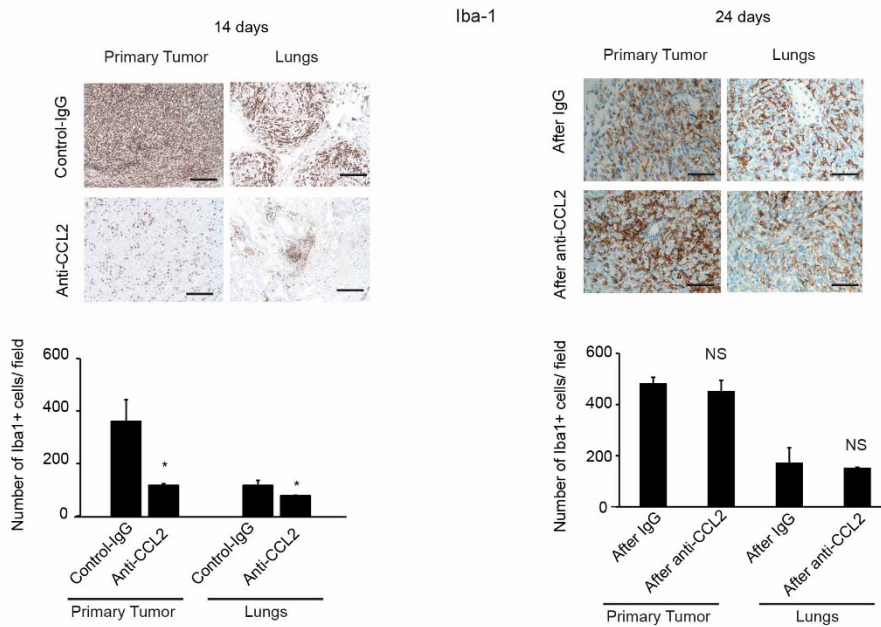
Extended Data Figure 6 | Distribution of inflammatory monocytes assessed by flow cytometry during and after treatment *in vivo*. a, Top, quantification of Ly6C$^+$Gr1$^+$ monocytes as percentage of SSC^{low}CD11b$^+$ cells on day 14 of anti-CCL2 or IgG treatment and 10 days after treatment interruption in 4T1.2-tumour-bearing animals. Data are shown as means ± s.e.m., $n = 8$ mice, pooled data from two independent experiments. *$P < 0.05$, unpaired t-test. Bottom, quantification of total number of monocytes on day 14 of anti-CCL2 or IgG treatment and 10 days after treatment interruption in 4T1.2-tumour-bearing animals. Data are shown as means ± s.e.m., $n = 8$ mice, pooled data from two independent experiments. *$P < 0.05$, unpaired t-test. **b**, Top, quantification of monocytes as Ly6C$^+$Gr1$^+$ monocytes as percentage of SSC^{low}CD11b$^+$ cells on day 14 of anti-CCL2 or IgG treatment and 10 days after treatment interruption in Met-1-tumour-bearing animals. Data are shown as means ± s.e.m., $n = 8$ mice, pooled data from two independent experiments. *$P < 0.05$, unpaired

t-test. Bottom, quantification of total number of monocytes on day 14 of anti-CCL2 or IgG treatment and 10 days after treatment interruption in 4T1.2-tumour-bearing animals. Data are shown as means ± s.e.m., $n = 8$ mice, pooled data from two independent experiments. *$P < 0.05$, unpaired t-test. **c**, Top left, representative images of Iba1-stained lung and tumour sections on day 14 of treatment. Bottom left, quantification of Iba1 staining. Total numbers of Iba1-positive cells are shown ± s.e.m. of 10 fields of view on 3 lungs sections per animal, $n = 3$ mice per group. Top right, representative images of Iba1-stained lung and tumour sections 10 days after cessation of the treatment. Bottom right, quantification of Iba1 staining. Total numbers of Iba1-positive cells are shown ± s.e.m. of 10 fields of view on 3 lung sections per animal, $n = 3$ mice per group. *$P < 0.05$, ANOVA with post-hoc Bonferroni correction. Scale bar, 100 μm. One representative image out of 10 is shown per group. NS, not significant.

a

7 days of treatment

b

7 days after treatment
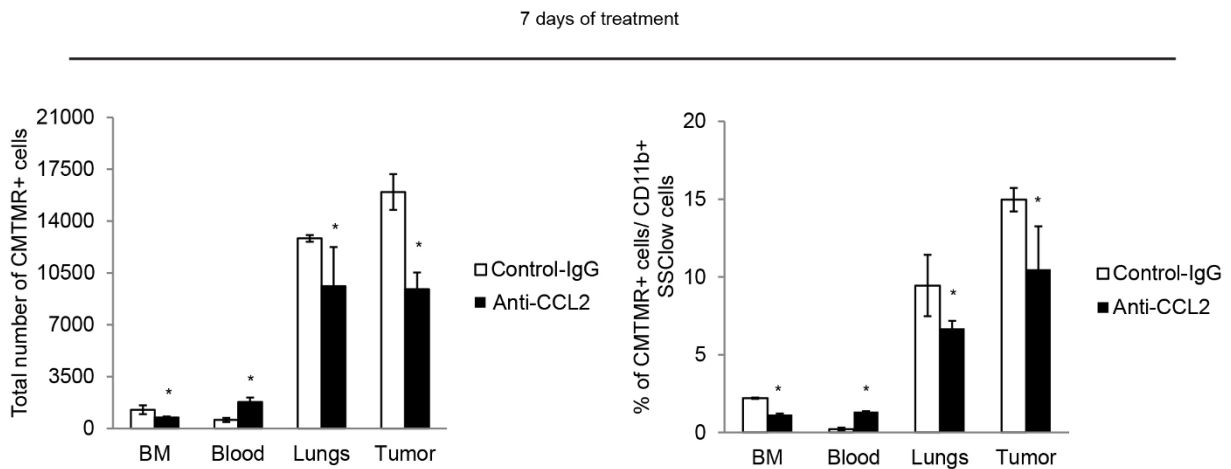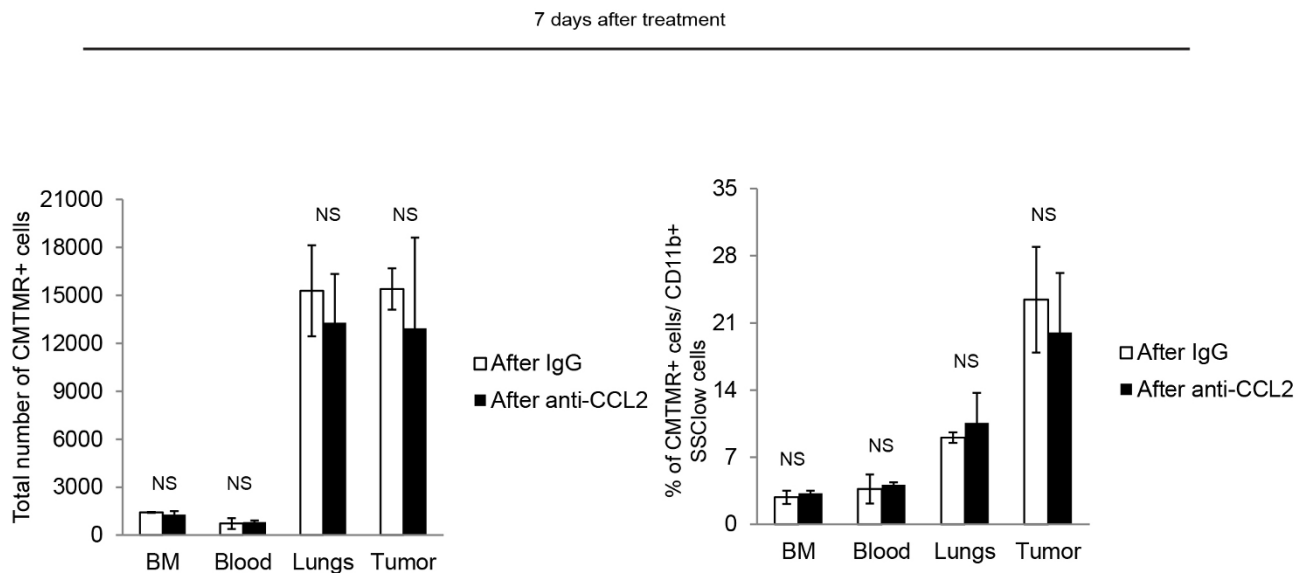
Extended Data Figure 7 | Recruitment of adoptively transferred CMTMR-labelled CCR2^{+} monocytes to the primary tumour and metastatic lung depends on CCL2. a, Quantification of adoptively transferred CMTMR^{+} monocytes as total numbers or percentages of SSC^{low}CD11b^{+} cells in different organs from tumour-bearing animals on day 7 of treatment. BM, bone marrow. Data are shown as means ± s.e.m., $n = 5$ mice per group, one representative of two independent experiments. *$P < 0.05$, unpaired t-test. **b**, Quantification of adoptively transferred CMTMR^{+} monocytes as total numbers or percentages of SSC^{low}CD11b^{+} cells in different organs from tumour-bearing animals on day 7 after interruption of the treatments. Data are shown as means ± s.e.m., $n = 3$ mice per group, one representative of two independent experiments. *$P < 0.05$, unpaired t-test. NS, not significant.

a

b

c

□ Control-IgG ■ Anti-CCL2

d

e
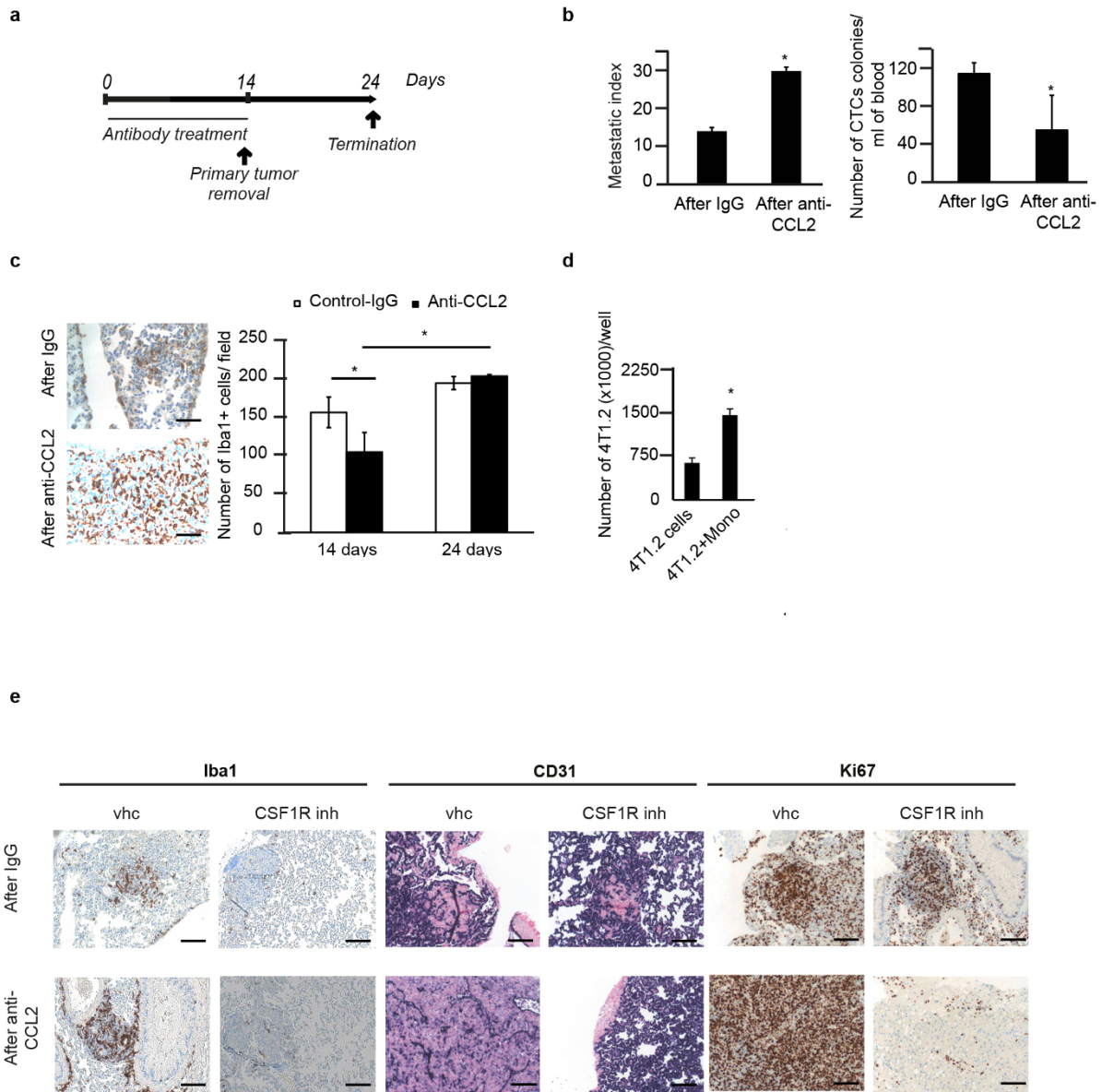
Extended Data Figure 8 | Monocytes support growth of tumour cells *in vivo* and *in vitro*. a, Timeline of the experiments. **b**, Left, metastatic index in lungs from 4T1.2-tumour-bearing animals on day 24. Data are shown as means ± s.e.m., $n = 4$ mice per group, one representative of two independent experiments. *$P < 0.05$, unpaired *t*-test. Scale bar, 100 μm. Right, the number of tumour cell colonies per ml blood of tumour-bearing animals on day 24 and after removal of the primary tumour. Data are shown as means ± s.e.m., $n = 4$ mice per group, one representative of two independent experiments. *$P < 0.05$, unpaired *t*-test. **c**, Left, representative images of Iba1-stained lung sections in animals treated as in Extended Data Fig. 8a. Right, quantification of Iba1 staining on day 14 (last day of treatment and the day of tumour removal)

and on day 24 (10 days after stopping treatment and tumour removal). Total numbers of Iba1-positive cells are shown ± s.e.m. of 10 fields of view on 3 lungs sections per animal, $n = 3$ mice per group. *$P < 0.05$, unpaired *t*-test. Scale bar, 100 μm. One representative image out of 10 is shown per group. **d**, Quantification of 4T1.2 cell viability using Trypan Blue 48 h after co-culture with sorted monocytes (Mono). Data are shown as means ± s.e.m., $n = 3$. *$P < 0.05$, unpaired *t*-test. **e**, Representative images of Iba1, CD31 and Ki67 staining of lung sections from animals treated with CSF1R inhibitor (CSF1Rinh) or vehicle (vhc) after treatment with anti-CCL2 or IgG control. One representative image out of 10 is shown per group.
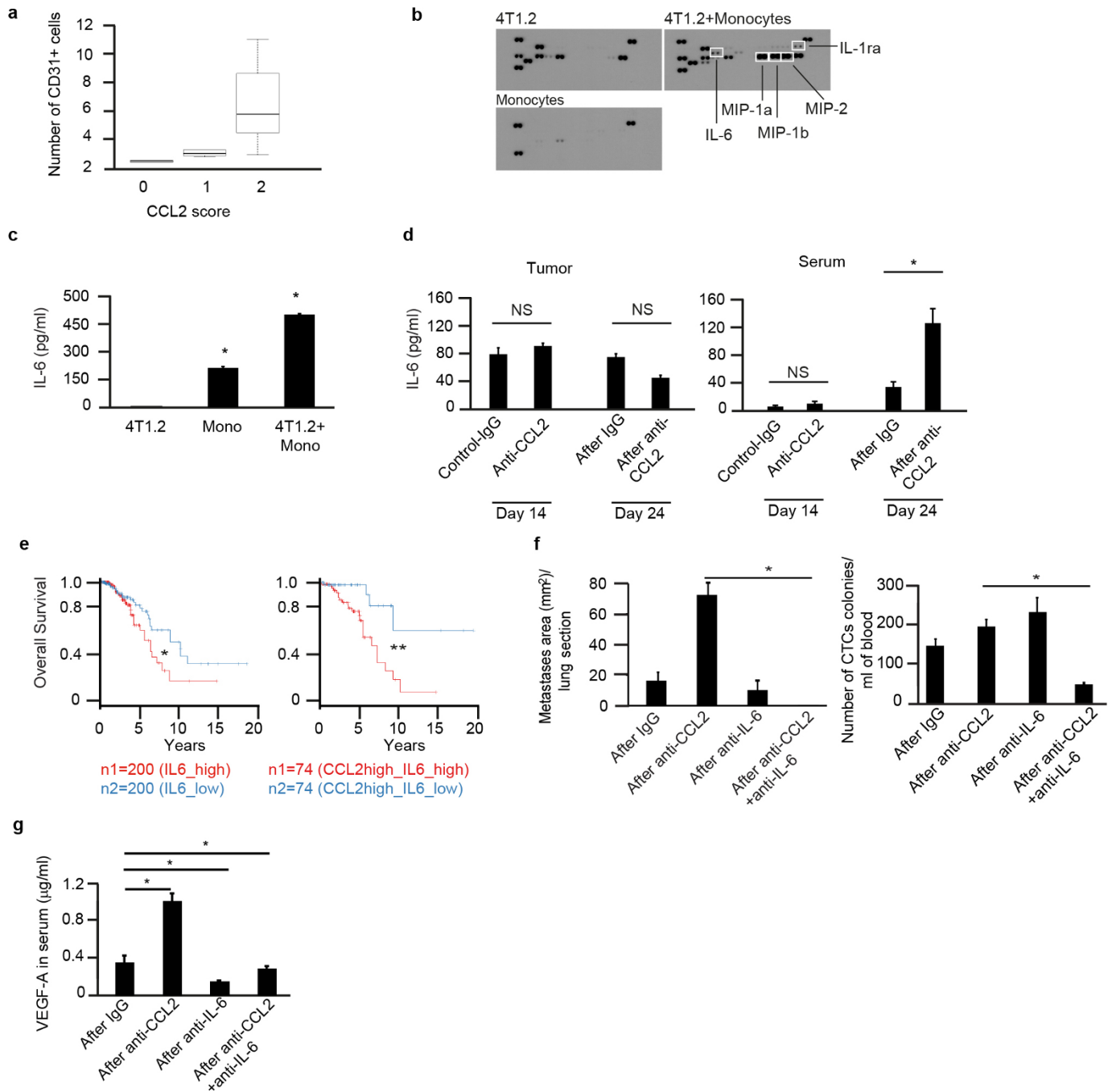
**Extended Data Figure 9 | Upregulation of CCL2 and IL-6 reduces overall survival in breast cancer patients. a,** Correlation between immunohistochemical score of CCL2 and number of CD31$^+$ vessels per high-power field in biopsies from patients with breast carcinoma ($n = 17$), $P = 0.031$. Data were analysed using R with one-way ANOVA (assuming that the data are normally distributed). The box plot represents the first to the third quartile of the data. Thick line indicates median, the whiskers in the box plot extend to the minimal and maximal values. **b,** Cytokine array showing expression of IL-6 in the supernatant of mono- or co-cultures of 4T1.2 cells and primary monocytes, in the presence or absence of anti-CCL2. **c,** Quantification of IL-6 expression in cell supernatants of monocytes in mono- or co-culture with 4T1.2 by ELISA. Data are shown as means ± s.e.m., $n = 4$ independent experiments each with biological triplicates. *$P < 0.05$, ANOVA with post-hoc Bonferroni correction. **d,** IL-6 expression levels in primary tumours (left) or in serum (right) on day 14 of treatment and after cessation of treatment (day 24). Data are shown as means ± s.e.m., $n = 6$ mice per group, pooled data from two

independent experiments. *$P < 0.05$, ANOVA with post-hoc Bonferroni correction. **e,** Left, Kaplan–Meier survival curves showing overall survival of 400 breast tumour patients expressing either low (blue) or high (red) IL-6 levels. *$P < 0.045$, log-rank test. Right, Kaplan–Meier survival curves showing overall survival of 148 patients with tumours expressing either CCL2 high/IL-6 low (blue) or CCL2 high/IL-6 high (red) levels. *$P < 0.0017$, log-rank test. **f,** Left, quantification of lung metastases. Metastatic area per lung section is shown ± s.e.m. of 20 fields of view on 5 lungs sections per animal, $n = 4$ mice per group. *$P < 0.05$, ANOVA with post-hoc Bonferroni correction. Right, number of colonies formed by CTCs per ml blood in animals treated as in Fig. 3c on day 24. Data are shown as means ± s.e.m., $n = 10$ mice per group, pooled data from two experiments. *$P < 0.05$, ANOVA with post-hoc Bonferroni correction. **g,** VEGF-A expression as measured by ELISA in serum from 4T1.2-tumour-bearing animals treated as in Fig. 3c. Data are shown as means ± s.e.m., $n = 4$ mice per group, pooled data from two experiments. *$P < 0.05$, ANOVA with post-hoc Bonferroni correction. NS, not significant.

a
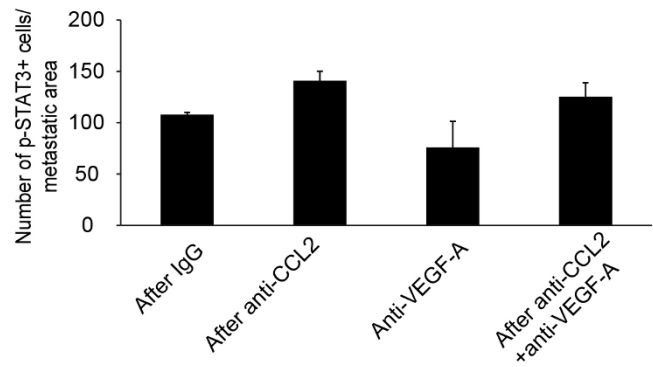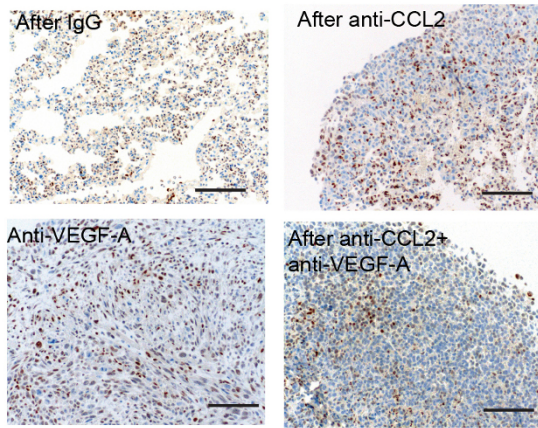
b
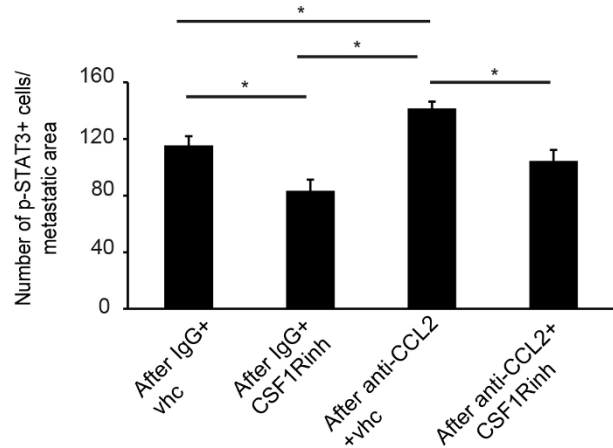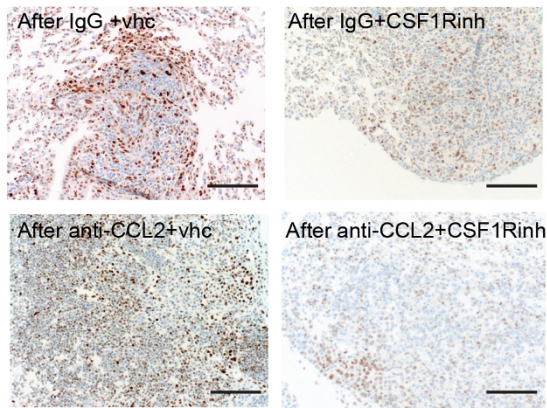
Extended Data Figure 10 | Monocytes/macrophages induce p-STAT3 in metastatic lungs upstream of VEGF-A expression. **a**, Left, representative images of p-STAT3-stained lung sections from animals treated as in Fig. 4a. Scale bar, 100 μm. Right, quantification of p-STAT3 staining. Total numbers of p-STAT3-positive cells per field are shown ± s.e.m. of 10 fields of view on 3 lungs sections per animal, $n = 3$ mice per group. **b**, Left, representative images

of p-STAT3-stained lung sections from animals treated as in Fig. 2c. Scale bar, 100 μm. Right, quantification of p-STAT3 staining. Total numbers of p-STAT3-positive cells per field are shown ± s.e.m. of 10 fields of view on 3 lungs sections per animal, $n = 3$ mice per group. CSF1Rinh, CSF1R inhibitor; vhc, vehicle. *$P < 0.05$, ANOVA with post-hoc Bonferroni correction. **a**, **b**, One representative image out of 10 is shown per group.